



**HAL**  
open science

# **A Numerical Study of the Behaviour and Failure Modes of Axially Compressed Steel Columns Subjected to Transverse Impact**

H. Al Thairy, Y.C. Wang

► **To cite this version:**

H. Al Thairy, Y.C. Wang. A Numerical Study of the Behaviour and Failure Modes of Axially Compressed Steel Columns Subjected to Transverse Impact. *International Journal of Impact Engineering*, 2011, <10.1016/j.ijimpeng.2011.03.005>. <hal-00829114>

**HAL Id: hal-00829114**

**<https://hal.science/hal-00829114v1>**

Submitted on 2 Jun 2013

**HAL** is a multi-disciplinary open access archive for the deposit and dissemination of scientific research documents, whether they are published or not. The documents may come from teaching and research institutions in France or abroad, or from public or private research centers.

L'archive ouverte pluridisciplinaire **HAL**, est destinée au dépôt et à la diffusion de documents scientifiques de niveau recherche, publiés ou non, émanant des établissements d'enseignement et de recherche français ou étrangers, des laboratoires publics ou privés.



HAL Authorization

# Accepted Manuscript

Title: A Numerical Study of the Behaviour and Failure Modes of Axially Compressed Steel Columns Subjected to Transverse Impact

Authors: H. AL Thairy, Y.C. Wang

PII: S0734-743X(11)00058-3

DOI: [10.1016/j.ijimpeng.2011.03.005](https://doi.org/10.1016/j.ijimpeng.2011.03.005)

Reference: IE 1987

To appear in: *International Journal of Impact Engineering*

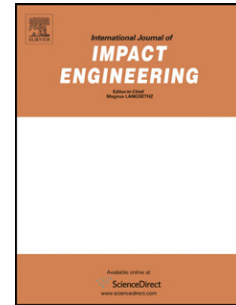
Received Date: 21 October 2010

Revised Date: 15 March 2011

Accepted Date: 17 March 2011

Please cite this article as: AL Thairy H, Wang YC. A Numerical Study of the Behaviour and Failure Modes of Axially Compressed Steel Columns Subjected to Transverse Impact, *International Journal of Impact Engineering* (2011), doi: 10.1016/j.ijimpeng.2011.03.005

This is a PDF file of an unedited manuscript that has been accepted for publication. As a service to our customers we are providing this early version of the manuscript. The manuscript will undergo copyediting, typesetting, and review of the resulting proof before it is published in its final form. Please note that during the production process errors may be discovered which could affect the content, and all legal disclaimers that apply to the journal pertain.



# A Numerical Study of the Behaviour and Failure Modes of Axially Compressed Steel Columns Subjected to Transverse Impact

H. AL-THAIRY<sup>1</sup>, Y.C. WANG\*

School of Mechanical, Aerospace and Civil Engineering, The University of Manchester, UK

\*Corresponding author, email: [yong.wang@manchester.ac.uk](mailto:yong.wang@manchester.ac.uk)

## ABSTRACT

In this study a numerical simulation of the behaviour and failure modes of axially compressed steel column subjected to transverse impact by a rigid mass at different impact speeds and locations is presented. Firstly, the capability of the present numerical model to trace the response and to predict different failure modes of transversely impacted beams and columns with and without axial compressive force has been validated. These failure modes include plastic global failure, tensile tearing failure and transverse shear failure. The validation was performed by comparing simulation results in term of the contact force, deformation shape, failure mode and the maximum transverse displacement with available published experimental test results by others. The progressive damage and failure model available in ABAQUS/Explicit has been utilized in the present numerical models to account for material shear and tensile tearing failure under impact. Comparisons between the experimental and simulation results confirmed that the numerical models were able to accurately predict the aforementioned failure modes. Thereafter, a parametric study has been conducted to investigate the effects of several parameters on the response of axially loaded steel column, based on the results of which simplifying assumptions on column behaviour under impact can be made to develop appropriate design calculation methods for steel columns under such loading conditions.

Keywords: impact, steel columns, numerical modelling, failure modes

## 1. INTRODUCTION

Columns in underground and multi-storey car parks, on the ground floor in buildings located along busy roads [1] or as bridge piers [2], are structural members which are highly vulnerable to impact loads due to moving vehicles. Catastrophic progressive structural failure may occur as a consequence of an accidental vehicle impact on such columns. A proper analysis technique that can take into account column failure under impact is required for rational column design. At present, there is little guidance on how to design this type of structural elements for impact resistance. In particular, the simplified analysis methods used in current codes and standards [3,4,5 and 6] generally deal with transverse impact by using an equivalent static lateral load, which can be grossly inaccurate.

A considerable amount of literature has been published on studies of the behaviour and failure modes of beams under transverse impact. In particular, the behaviour of axially restrained beams under transverse impact has been studied intensively [7, 8, 9, 10, 11, 12, 13 and 14]. This is understandable since axially restrained beams are frequently used as members to absorb impact energy in such major applications as vehicle crash barriers. On the other hand, although columns under compressive load may also be involved in accidental vehicle crash, the emphasis has been almost wholly on vehicle crashworthiness for occupant protection. However, with structural robustness now an important topic for the structural engineering research community, the behaviour of columns under vehicle impact deserves attention. Nevertheless, although the behaviour of axially compressed columns under transverse impact

will be different from that of axially restrained beams undergoing axial tension, a review of beam behaviour can help understand some aspects of the column behaviour.

The experimental results of Meknes and Opat [7] identified three modes of failure of clamped beams subjected to transverse impulsive dynamic load: (i) large plastic deformation of the whole beam with the formation of a plastic hinge mechanism; (ii) tensile tearing failure under catenary action; (iii) and transverse shear failure at the supports. A large number of research studies have investigated how these three failure modes may be quantified under the influence of different parameters, such as material type and impact location [8, 9, 10, and 11], axial pre-loading [12], the impact speed [13], and different types of cross-section [14]. Of these three failure modes, global failure and shear failure may occur in axially compressed columns under transverse impact.

Among a few studies on behaviour of axially compressed columns under transverse impact, Zeinoddini et al [15 and 16] carried out an experimental and numerical investigation to study the response of axially pre-compressed steel tubes under low velocity transverse impact. Two failure modes were identified: plastic global buckling under high axial compression, and local indentation and damage of the impact zone when the axial load is low and the tube is thin. Crucially, their study indicated that quasi-static analysis may be used for the impact velocity used. Adachi et al [17] and Sastranegara et al [18] investigated experimentally and numerically the buckling and post buckling behaviour of axially compressed aluminium columns subjected to lateral impact loads. They also identified global instability as the main failure mode of the columns. Due to the failure mode being global buckling, they found that the critical condition of column buckling was controlled only by the kinetic energy of the

transverse impact, but independent of the history of the transverse impact or its impulse. These experimental results also provide data for validation of numerical and analytical modelling.

Typically, since the above studies are among the first on this topic, they are limited in scope and their conclusions are preliminary. Consequently, there is insufficient data to develop comprehensive understanding of the effects of various parameters on column behaviour for the development of practical design methods. The aim of this research is to build on these preliminary research investigations and develop an extensive database of column behaviour under transverse impact. Specifically, the objectives of this paper are as follows:

- (1) to validate a method of numerical simulation for the behaviour and failure modes of axially compressed steel columns subjected to transverse impact caused by a rigid mass travelling at relatively low velocity. The simulations will be carried out using the general finite element code ABAQUS/Explicit [20];
- (2) using the validated numerical model, to investigate the effects of several parameters on the response and failure modes of the impacted column.

## **2. VALIDATION OF THE NUMERICAL MODEL**

In this section, the capability of the ABAQUS/Explicit model to accurately follow the response and predict different failure modes of axially compressed steel columns under transverse impact will be assessed against three series of published experimental tests. These three series of experiments were selected to ensure that different possible column failure modes would be covered.

## 2.1. Global plastic buckling failure

The tests were conducted by Zeinoddini et al [15]. In these tests, the steel tube was one metre length; it was pre-compressed and then impacted at the mid point using a drop weight of 25.45 kg with a falling velocity of about 7 m/s (about 25 km/hour). The tubes were loaded to different levels of axial compression. The test set up is shown in Figure 1 together with the present ABAQUS model of the steel tube. The steel tube was modelled using linear three dimensional four-node doubly curved shell elements with reduced integration and membrane strain effects (S4R). The impactor was modelled using three dimensional 8-node brick element (C3D8R) with reduced integration and hourglass control. Classical metal plasticity model available in ABAQUS/Explicit was used for the steel tube. The density and modulus of elasticity for the steel tube were taken to be  $7850 \text{ kg/m}^3$  and  $200000 \text{ N/mm}^2$  respectively [15]. The input yield stress of the steel tube was  $500 \text{ N/mm}^2$  with Poisson's ratio was 0.3 [15].

The contact pair algorithm available in ABAQUS/Explicit was used to simulate the contact interaction between the impacting mass and the steel tube. In this algorithm, the hard contact and penalty formulation were used to describe normal and tangential behaviours respectively as mechanical interaction properties. Kinematic contact enforcement method was adopted to detect contact between the two bodies with small sliding formulation. A linear spring was used to apply the axial compressive load, as shown in Figure 1. The linear spring is attached to the sliding end of the tube to account for the decrease in axial force in the test due to movement of the end towards the clamped end [15]. It should be pointed out that because ABAQUS/Explicit was used only to conduct dynamic rather than static analysis, the axial

compressive load was applied using a special quasi-static analysis procedure in which the load was applied during the natural period of the system by utilizing a smooth amplitude step [19].

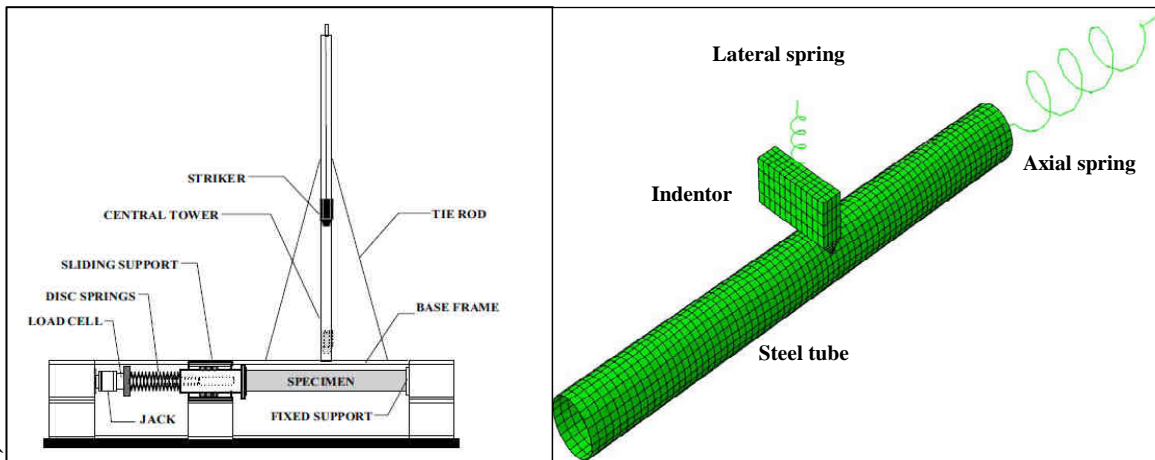


Figure 1: Experimental set up of Zeinoddini et al [15], left and Present numerical model, right

The experimental results indicated global column failure in columns with axial load value above 65% of the tube squash-load [15]. In this failure mode, the column lost its stability and large lateral deformations developed causing the column to shorten and slide towards the fixed end. For lower axial load ratios, no global failure occurred but local and plastic deformations and indentations were recorded at the impact zone [15, 16]. In the present numerical model, global failure was predicted at axial load ratio of 60% of the tube squash load as shown in Figure 2, which is about 93 % of the experimental value. For the other axial load values, there was no column failure, which conforms to the experimental results. Figure 3 compares the recorded and simulated impact force – time relationships for different axial load ratios. The agreement is very good.

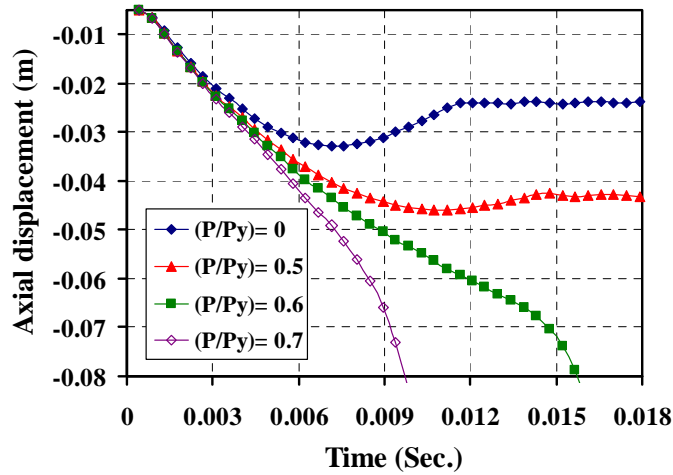


Figure 2: Axial displacement - time history of the impacted steel tube for different axial load levels

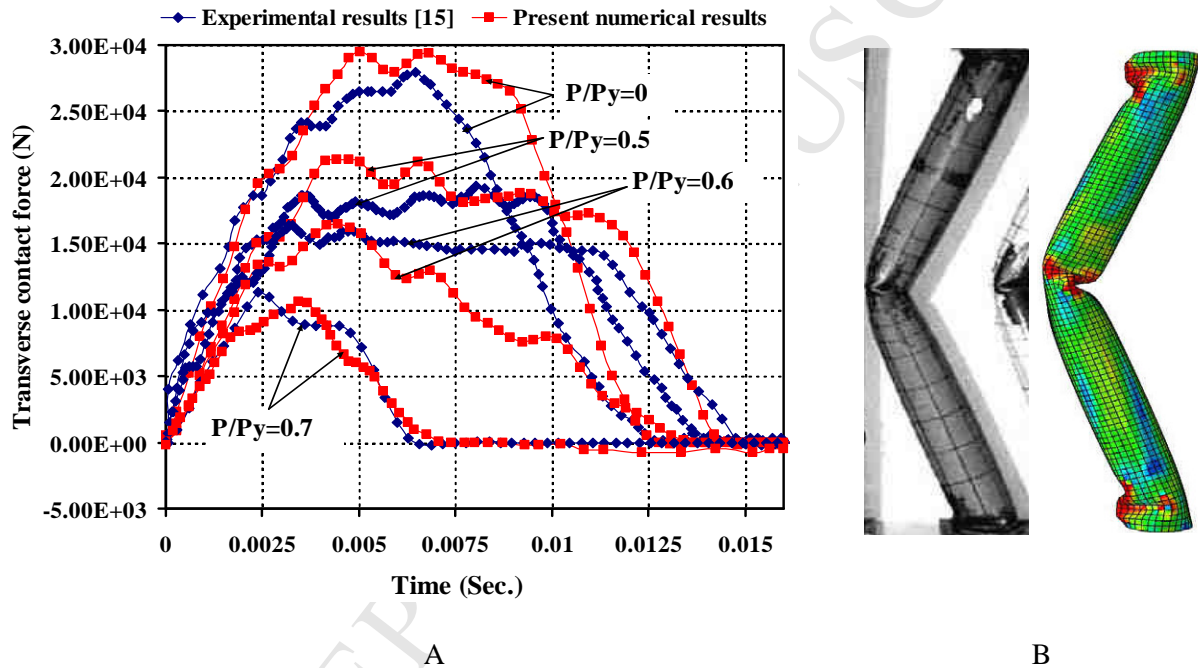


Figure 3: Comparison of the contact force (A), and deformation shape for (P/Py)=0.6 (B) for the tests of Zeinoddini et al [15]

## 2.2. Tensile tearing failure

Bambach et al. [14] performed the tests on 700mm long clamped steel hollow section sizes 50SHS impacted laterally by 600 kg mass falling with a velocity of 6.2 m/s. Figure 4 shows details of the experimental specimen together with the FE simulation model. There was no axial load in the specimens.

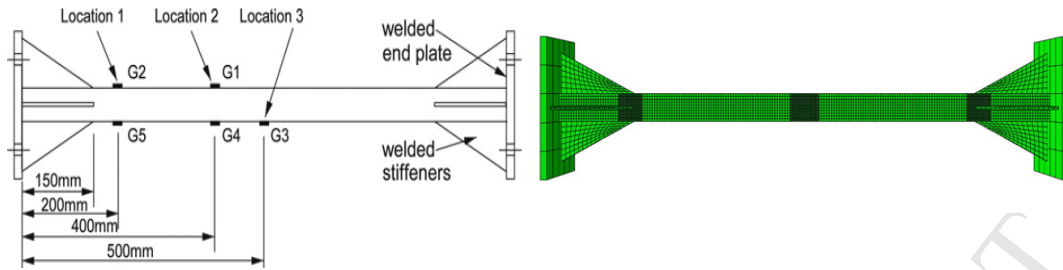


Figure 4: Experimental specimen of 50SHS [14], left and Numerical model, right

The same simulation methodology (element type for the hollow section, element type for the impactor, contact interaction) as in section 2.1 was used.

The material behaviour of the hollow section and the gusset plates (**C350 steel**) were simulated using the classical metal plasticity model in conjunction with the progressive ductile damage and failure model available in ABAQUS/Explicit to simulate tensile failure. Isotropic strain hardening and strain rate effect were accounted for by utilizing the true stress–true strain curve provided from the experiment [14]. No plastic behaviour was included in the material behaviour models of the impactor and the supporting gusset plates because they did not show any sign of deformation during the impact test. The steel density was  $7850 \text{ kg/m}^3$  and modulus of elasticity  $200000 \text{ N/mm}^2$ . The engineering yield stress for the tube was  $455 \text{ N/mm}^2$  and the Poisson's ratio was 0.3 [14]. Material strain rate sensitivity was taken into account by employing the Cowper-Symonds equation with  $D= 40.4$  and  $q=5$  according to the experimental results reported in [19]. Table 1 gives the true stress-strain values.

Table 1: Material properties for C350 used in numerical simulation [14]

Section dimension (mm)	Beam length(mm)	True yield stress $\text{N/mm}^2$	True ultimate stress $\text{N/mm}^2$	True failure strain%
$50 \times 50 \times 1.6$	700	456	584.64	0.145

### 2.2.1 Modelling of tensile failure

The progressive damage and failure model provided in ABAQUS/Explicit has been employed in the present model to detect and trace the damage initiation and evolution until complete failure of the material at integration points of the element. The model uses the equivalent plastic strain at the onset of damage  $\varepsilon_D^{pl}$  as failure initiation criterion. The value of this strain can be input as tabular fraction of the strain rate and stress triaxiality, which is defined as the ratio of the pressure stress to the equivalent Mises stress [20]. Material degradation starts when the damage initiation criterion is met based on the following condition:

$$\Phi_f = \frac{\sum \Delta \varepsilon^{pl}}{\varepsilon_D^{pl}} = 1 \quad (1)$$

where  $\sum \Delta \varepsilon^{pl}$  is the accumulative value of the equivalent plastic strain at integration points.

The fracture strain at ductile damage initiation was first obtained from the stress vs. plastic strain data [20], obtained from the uni-axial tensile test of the beam material C350 (=0.115 in this case). Then, a nonlinear FE analysis was performed on the impacted hollow steel beam under same loading conditions but using the classical metal plasticity constitutive model to obtain values of maximum stress triaxiality and strain rate at damage initiation. The values of these quantities together with values of other material failure quantities used in the present numerical model are shown in Table 2.

Once damage initiation has been detected, the damage process continues and the damage evolution can be traced assuming a linear relationship of the damage variable with effective plastic displacement, [20]. The damage variable represents the accumulated ratio of the

effective plastic displacement  $u^{pl}$  at integration points to the total plastic displacement at the point of failure (full degradation),  $u_f^{pl}$ , Table 2.

$$\dot{d} = \frac{\dot{u}^{pl}}{u_f^{pl}} \quad (2)$$

The effective plastic displacement,  $u^{pl}$ , is defined with the following evolution equations:

$$\dot{u}^{pl} = L \dot{\epsilon}^{pl} \quad (3)$$

$$u_f^{pl} = L \epsilon_f^{pl} \quad (4)$$

Where  $L$  is the characteristics length of the element defined in the current model as the square root of the integration point area, [ABAQUS/user manual, 20].  $\epsilon_f^{pl}$  is the equivalent plastic strain at complete failure of the material taken from the uni-axial stress strain curve, Table 2.

Using effective plastic displacement as damage evolution criterion helps to reduce mesh dependency of the results [20]. According to the mesh size used in the numerical model for this test, the value of  $L$  is assumed to be 2 mm. The value of the damage variable  $d^*$  ranges from 0 corresponding to damage initiation stage to 1 representing complete failure. When complete failure occurs ( $d^*=1$ ), ABAQUS/Explicit offers two procedures to complete the analysis: either removing the failed element from the model mesh or keeping it but setting its stress to zero in next analysis step. The first option was used in the present numerical simulation

Table 2: Material failure parameters used in the present numerical model

Fracture strain	Maximum stress triaxiality.	Maximum strain rate (s <sup>-1</sup> )	$\epsilon_f^{pl}$	$u_f^{pl}$ (m)
0.115	0.7	14.2	0.1455	0.000291

### 2.2.2 Simulation results

Table 3 and Figure 5 compare the experimental and the numerical simulation results in term of the peak contact force (Table 3) and the failure mode (Figure 5). Table 3 indicate close correlation for the peak contact force and Figure 5 shows accurate simulation of complete tensile tearing failure of the beam section at the supports.

Table 3: Comparison of contact force between experimental result [14] and numerical simulation

Source of results	Peak contact force
Experimental Result [14]	40.5 kN
Present numerical results	45 kN

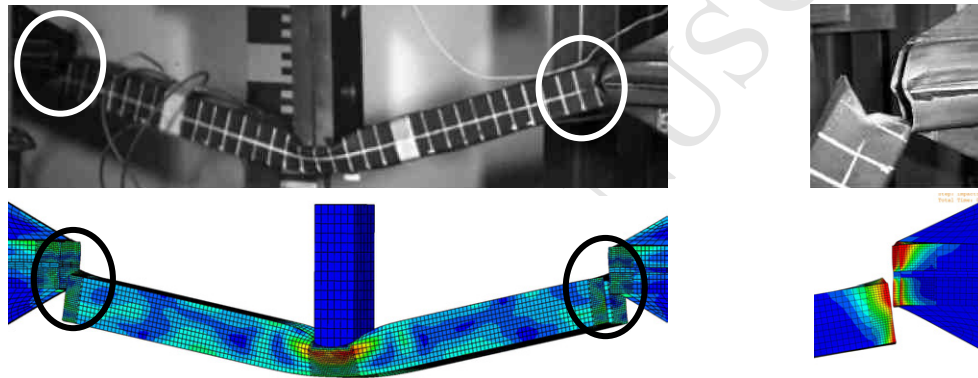


Figure 5: Deformation shape and tensile fracture at the supports at 20 ms after impact, Top: experimental result [14], Bottom: numerical simulation

Figures 6 plots the damage initiation profiles at different times and shows that the damage initiation criterion was satisfied at the supports only by reaching the maximum value of 1. Figure 7 compares damage evolution between the supports and the impact point. While the impact region experienced higher damage initially due to direct contact, the supports experienced drastic increase in damage due to lateral deformation of the structural member inducing large axial tensile stress at around 8 ms.

Form comparison between experimental and simulation results, it can be concluded that the damage initiation and failure criteria have been employed correctly in the present model to simulate material failure under tension.

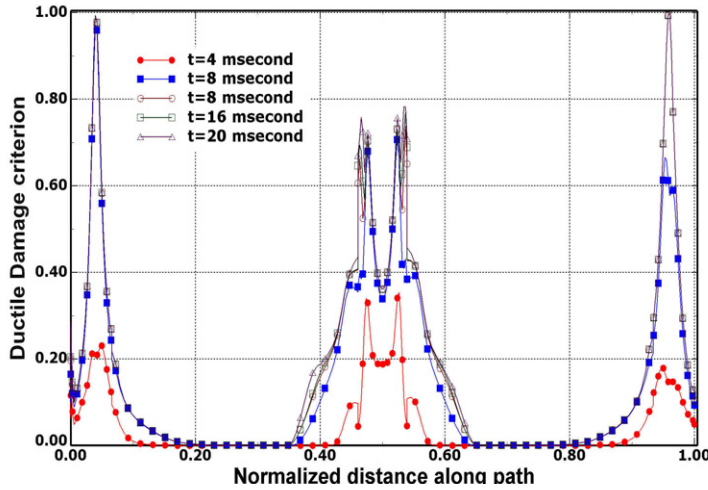


Figure 6: Ductile damage initiation profile along the top surface of the beam

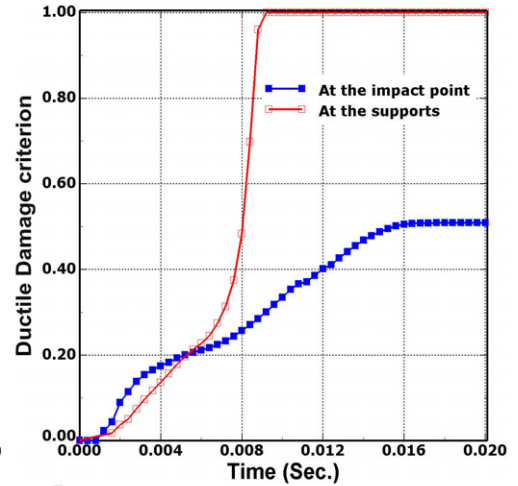


Figure 7: Ductile damage initiation history of the top surface at the support and the impact point

### 2.3. Shear failure

The experiments were conducted by Yu and Jones [11] on a mild steel beam of solid rectangular cross-section ( $B \times H = 10.13 \times 6.2 \text{ mm}$ ) with clamped ends and 101.6 mm in clear span. The clamped length of each end was 50.8 mm to ensure full fixity. The steel beam was impacted transversely at a distance of 49.9 mm from the left support by a rigid mass of 5kg with a velocity of 10.6 m/s.

ABAQUS brick element C3D8R was used, as in previous models, to simulate both the solid beam and the impactor. The beam's element size was 2.5 mm based on mesh sensitivity check. As shown in Figure 8, the size of the elements was reduced near the impact zone and the supports to be 0.5 and 1 mm respectively to ensure accurate simulation of nonlinear behaviour, contact interaction and shear failure path. Figure 9 shows the mild steel true stress-

strain relationship, based on the classical metal (Mises) plasticity model available in ABAQUS/Explicit with isotropic strain hardening and strain rate effects. The strain rate effects were described by employing the Cowper-Symonds equation with material parameters  $D=1.05 \times 10^7 \text{ s}^{-1}$  and  $q = 8.3$  [11, 12]. These values of  $D$  and  $q$  were chosen by Liu and Jones [11] to describe the strain rate-sensitive behaviour of the steel material based on experimental results. The same contact interaction model as in the previous simulations was used to simulate contact between the rigid mass and the solid beam except that in the current model, the tangential behaviour of the contact was assumed frictionless, based on the experimental observation that slipping occurred during the tests between the impacting mass and the steel beam at the impact zone [11]. Other properties (steel density, modulus of elasticity and Poisson's ration) were the same as in previous simulations.

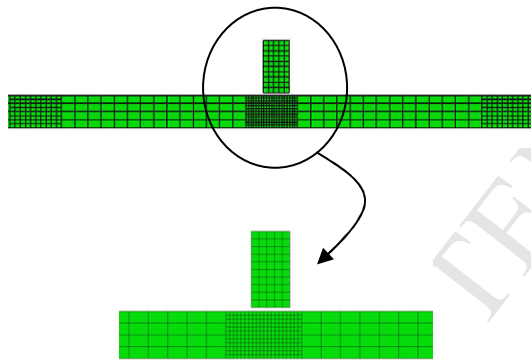


Figure 8: FE model and mesh size of the steel beam with a close-up view of the mesh at the impact point

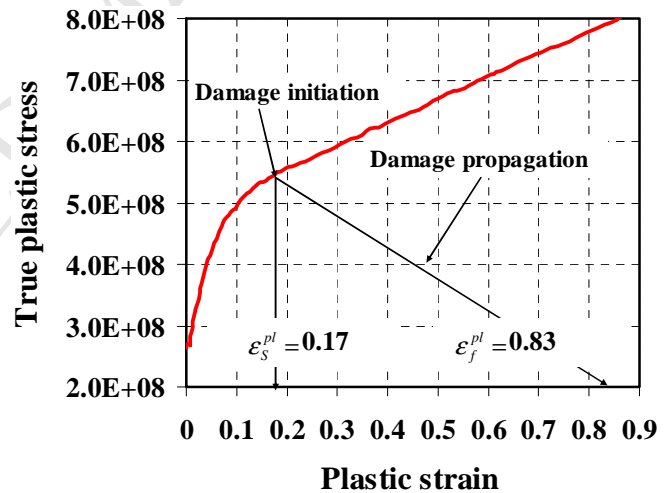


Figure 9: True stress-True strain curve used to model the steel plastic behaviour

### 2.3.1 Modelling of shear failure

The same progressive damage and failure model as described in section 2.2.1 was used except that the damage initiation criterion would be described here in term of the equivalent plastic

strain at the onset of shear damage ( $\epsilon_s^{pl}$ ). Shear damage is assumed to propagate when the following condition is satisfied:

$$\Phi_s = \frac{\sum \Delta \epsilon^{pl}}{\epsilon_s^{pl}} = 1 \quad (5)$$

where  $\sum \Delta \epsilon^{pl}$  is the accumulative value of the equivalent plastic strain at integration points.

The values of maximum shear stress ratio and strain rate at the onset of failure were obtained by first performing a nonlinear FE analysis using the classical metal plasticity model. Table 4 provides values of these quantities together with other values of material failure quantities used in the present numerical. The damage progress was traced using a linear damage evolution variable with effective plastic displacement  $u_f^{pl}$  based on the value of the equivalent plastic strain at failure point  $\epsilon_f^{pl}$  as described in the previous section. Table 4 presents the values of these quantities used in the simulation.

. Table 4: Material failure parameters used in the present numerical model

Fracture strain	Maximum shear stress ratio	Maximum strain rate (scc <sup>-1</sup> )	$\epsilon_f^{pl}$	$u_f^{pl}$ (m)
0.172	1.8	320	0.83	0.000415

### 2.3.2 Simulation results

Figure 10 shows the deformed shape of the impacted steel specimen after complete shear failure from both the test and the present numerical simulation. Good correlation can be seen between the two shapes in terms of the location and angle of the shear failure surface. Correlation between the results is highly satisfying. Table 5 compares the maximum permanent transverse deformation of the beam between the present numerical results, the experimental results of Liu and Jones [11] and the numerical results of Yu and Jones [12],

although it can be noted that the model of Yu and Jones [12] did not incorporate failure simulation. Figure 10 further compares the axial normal strain of the steel beam underneath the impact point obtained by the present numerical model with that recorded experimentally by Liu and Jones [11]. Excellent agreement can be noticed throughout. This exercise can be used to confirm the accuracy and efficiency of the present numerical model to simulate shear failure mode.

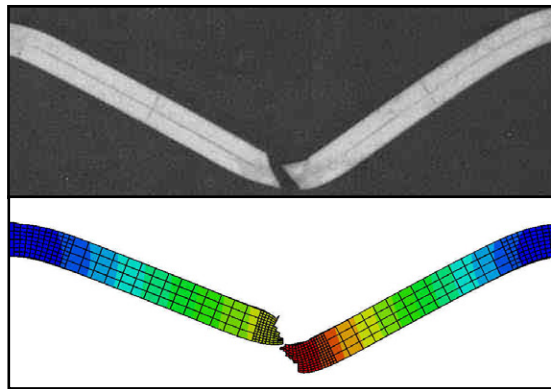


Figure 10: Comparison of the deformation shape of the steel specimen after shear failure between experimental test [11] (Top) and numerical simulation (Bottom).

Table 5: Comparison of the maximum transverse displacement between results from the present numerical simulation with the experiment results, of ref [11] and the numerical simulation results of ref [12]

Quantity	Experiment, [11]	Numerical, no failure criteria, [12]	Numerical, present study
maximum permanent transverse déformation (mm)	21.8	21.26	21.5

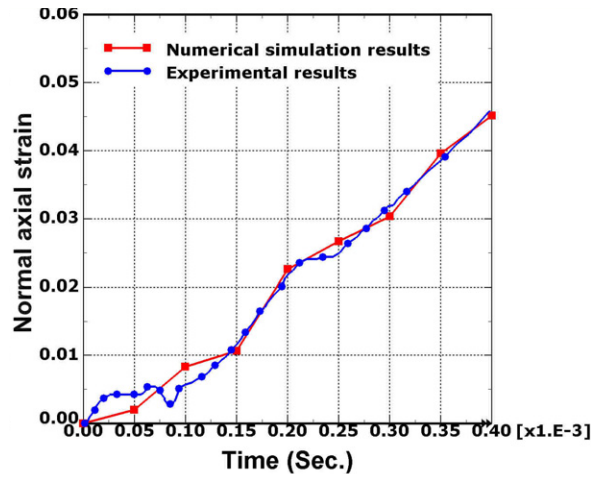


Figure 11: Comparison of axial strain on the lower surface underneath the striker between the experimental [11] and the present numerical simulation results

Figure 12 plots the numerical results of shear damage initiation criterion profiles along the beam length at the top and bottom surfaces. At the mid span where shear fracture occurred, the shear damage initiation criterion was satisfied for both surfaces; at the supports, shear failure had started but had not progressed through the entire section. This behaviour agrees with the experimental observation.

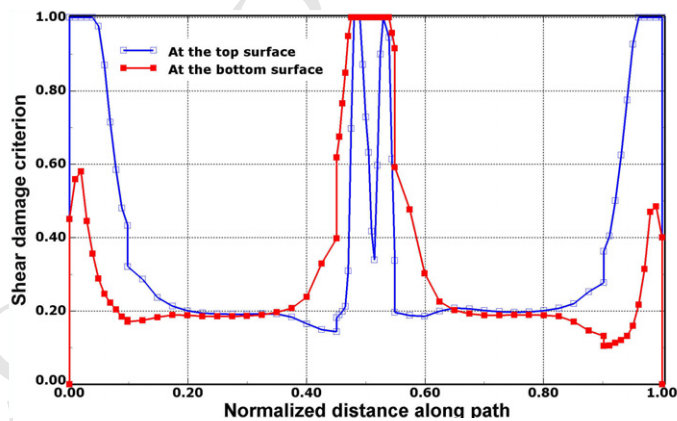


Figure 12: Shear damage initiation profile at the top and bottom surfaces of the beam along its length

As conclusion, it may be accepted that the present ABAQUS/Explicit model with the associated material behaviour and failure models is capable of simulating the behaviour and different failure modes of axially compressed columns under transverse impact.

### 3 PARAMETRIC STUDY

An important objective of this research is to develop thorough understanding of the effects of different parameters on the response and failure modes of axially compressed steel column under transverse impact. This can enable simple methods of analysis to be developed so that complicated numerical analyses such as employed in this research may be dispensed with in practical design procedure. Simplifying assumptions will be necessary when developing any design calculation method, and it is important that such assumptions are based on comprehensive understanding of the effects of different parameters on column behaviour and failure modes such that the limitations of these assumptions are clearly defined.

In this research, the following five important parameters have been identified for parametric study: impact velocity, impact location, axial compressive load, impactor mass and column slenderness ratio. This section will present numerical simulation results to help understand the effects of these design parameters.

The parametric study uses two simply supported H-section steel columns designed according to the British Standard BS 5950: Part 1:2000 [21] to resist a total load of 6800 kN or 3800 kN. These loads represent approximate total axial compressive loads exerted on the interior ground floor columns of 10 and 5 stories respectively of typical commercial steel buildings. To account for slenderness effect, two column lengths were used. Table 6 lists the column dimensions and slenderness.

Steel was assumed to be grade S355 and the steel modulus of elasticity and yield strength were assumed to be 206000 N/mm<sup>2</sup> and 355N/mm<sup>2</sup> respectively [21]. Full frontal impact was applied in the direction of the column flanges to cause bending about the weak (minor) direction (y-y axis) of the steel column, which represents one of the most critical cases for design purpose.

Table 6: Steel column dimensions and slenderness ratio

Column length( m)	Column section	Slenderness ratio $(\frac{kL}{r})_{y-y}$	Relative slenderness $\lambda_{y-y} = \frac{kL}{r\pi} \sqrt{\frac{F_y}{E}}$
4	UC 305×305×118	51.5	0.68
8	UC 356×406×340	76.9	1.02

### 3.1 Modelling properties

The same ABAQUS/Explicit simulation model as employed in the previous section was used, with the following mesh and material properties:

Strain rate effect: Cowper-Symonds equation with  $D=40.4 \text{ s}^{-1}$ ,  $q = 5$  [19]; Material failure properties: Figure 13 and Table 7. It should be mentioned that because this parametric study considered only columns with free axial movement, there would not be tensile tearing failure. Therefore, Table 7 only gives properties for simulating transverse shear failure;

A nonlinear finite element analysis was carried out to determine other failure quantities (maximum shear stress ratio, maximum strain rate), and these are presented in Table 7.

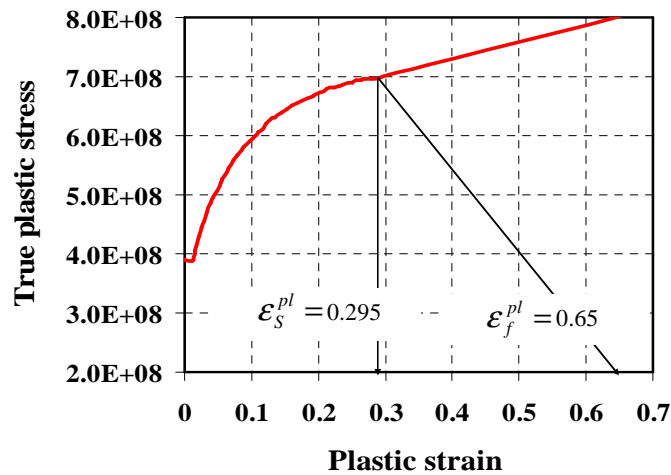


Figure 13: True stress –strain curve used to simulate S355 material behaviour in the parametric study

Table 7: Material failure parameters used in the parametric study

Fracture strain	Maximum shear stress ratio	Maximum strain rate (sec <sup>-1</sup> )	$\epsilon_f^{pl}$	$u_f^{pl}$ (m)
0.295	1.85	320	0.65	0.000415

### 3.2 Sequence of load application

Because ABAQUS/Explicit was used, the axial compressive load was applied first using a special quasi-static analysis procedure in which the axial load was applied to the column in a separate analysis step during the natural period of the column by utilizing a smooth amplitude step (ABAQUS parameters AMPLITUDE and SMOOTH STEP) [20]. After the column achieved equilibrium, the impact load was applied by establishing a contact interaction between the impacting mass and the steel column at the desired impact location.

### 3.3 The impactor mass:

Since the current study aims to investigate the behaviour and failure modes of axially loaded steel columns under transverse impact, the emphasis was on the column rather than the impactor. Therefore, only a brief description is given on the impactor. The impactor was assumed to be a cuboid rigid mass of dimensions  $1.5 \times 0.5 \times 0.3$ m as shown in Figure 14.

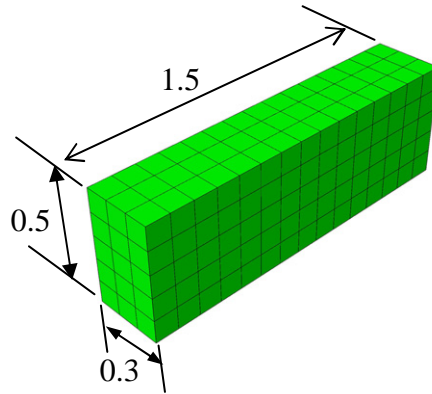


Figure: 14 Shape and dimensions of the impactor used in the parametric study

The modulus of elasticity of the impactor was selected to make it behave as an almost rigid body so that all kinetic energy of the impact would be absorbed by the steel column without any contribution from the impactor. The density of the impactor was adjusted to give the required mass. It will be shown in the parametric study results that for the highest impact velocity (80 km/h), only one column experienced shear damage at the impact zone due the sharp edges of the impactor. Therefore, the impactor shape was not considered to have significant effect on the column behaviour within the velocity range investigated in this study, which was 20 -80 km/s.

### 3.4 Mesh size sensitivity

Table 8 compares the FE simulation results using different element size against theoretical values [24] for natural frequency and buckling load of the UC 356×406×340 column with total length of 8 meter. The element sizes in Table 8 are all appropriate for static simulation. Figure 14(A) and 14(B) plot the column longitudinal movement and shear damage evolution at the impact point as function of time. It can be noticed from both figures that a mesh size

corresponding to 28845 elements (10 mm within one meter of the impact point and 50 mm for the rest of the column) can be adopted, Figure (15).

Table 8: Sensitivity of some static and dynamic results against the element size of the column model for the section UC 356×406×340 and length equals to meter

Element size (mm)	Frequency (cycles)	$P_{(buckling)} (\times 10^7 \text{ N})$
250	12.905	1.44561
100	12.960	1.45871
50	12.954	1.59895
20	12.958	1.59285
Theor. solution [24]	13.07	1.4884

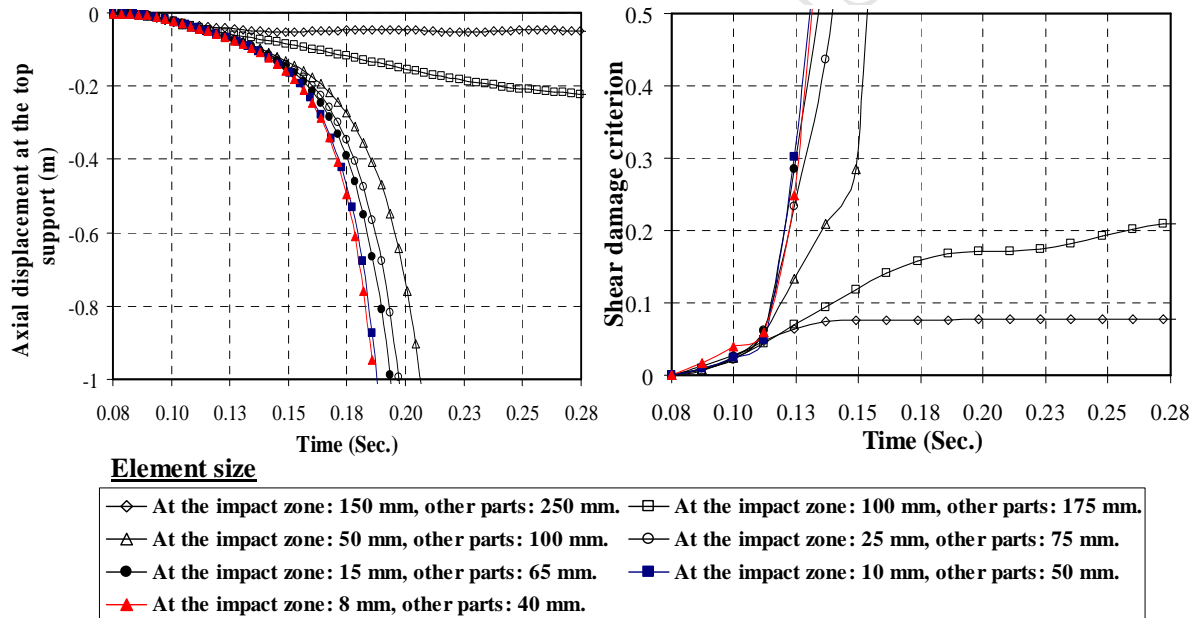
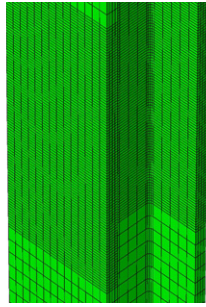
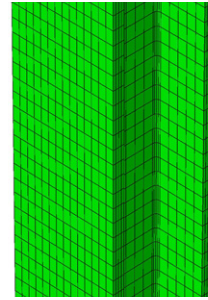


Figure 15: Sensitivity of column axial displacement history,  $V=40 \text{ m/s}$  (A) and shear damage history at the impact point,  $V=60 \text{ m/s}$  (B) for different mesh size, column section UC 356×406×340,  $P=50\%P_{Design}$ , Impacting mass=6 Ton.



(A) Impact zone (10mm)



(B) Rest of the column (50mm)

Figure 16: A closed-up view of the finite element mesh for the steel column model adopted in the parametric study

### 3.5 Analysis of results

Table 9 lists the parameters investigated in this study. These impact velocities may represent average velocities of vehicles passing through urban, residential and commercial areas. The different weights may represent those of a typical car, a light truck and a lorry.

Table 9: Parameters used in the numerical parametric study

Design Case	(P/P <sub>design</sub> )%	Impacting mass (Tons)	Impact velocity (km/h)	Impact location from bottom of column (m)
L=4 m UC 305×305×118	0, 0.3, 0.5, and 0.7	1.0, 3.0, and 6.0	20, 40 and 80	1.0 for M =1.0 and 3.0 Tons 1.5 for M = 3.0 and 6.0 Tons
L=8 m UC 356×406×340	0, 0.3, 0.5, and 0.7	1.0, 3.0, and 6.0	20, 40 and 80	1.0 for M =1.0 and 3.0 Tons 2 for M = 3.0 and 6.0 Tons

#### 3.5.1 Failure modes

Tables 10 and 11 present failure modes for the two different column sizes. It can be seen from these tables that global plastic buckling was the predominate failure mode except for the one case corresponding to the most heavily loaded ( $0.7P_{\text{Design}}$ ) stocky column (4m, UC 305×305×118) subjected to the most heavy mass impacting at the highest velocity of 80 km/h. This indicates that although shear damage may occur to axially compressed columns under lateral impact, the simulated scenario is unlikely to occur as it represents the very rare

case of high impact velocity/high impact mass/high axial load. Therefore this mode of failure (shear failure) may be ignored when developing the analytical approach for quantifying the critical failure conditions of steel columns in buildings located in urban areas.

For UC 305×305×118, Table 11 indicates that global plastic buckling was the predominate failure mode, but it was accompanied by local distortion in the flanges at the impact zone, particularly when the impact location was close to the column base ( $x=1\text{m}$ ), see Figure 15. This figure also shows that the severity of flange distortion increases with increasing axial load. However, detailed examination of column behaviour from the simulation models in terms of the deformed shape at different time intervals after the impact, Figure 17, confirms that flange distortion occurred after column global instability. For example, Figure 16 presents axial displacement – time history for two columns. Rapid acceleration of deformation of the columns at about  $t=45$  msec and  $t= 90$  msec indicates onset of column failure. Figure 17 shows deformed shapes of these two columns, indicating no significant local flange distortion at the corresponding times. This suggests that local flange distortion is a result, not the cause, of column global failure. Analysing column behaviour without considering local flange distortion would considerably simplify the analytical model.

Table 10: Failure modes for column section UC 356×406×340

L=8m, Impact location =2 m							L=8m, Impact Location =1m					
(P/P <sub>Design</sub> )%	Impact velocity (km/h)						Impact velocity (km/h)					
	20		40		80		20		40		80	
	Mass (Ton)		Mass (Ton)		Mass (Ton)		Mass (Ton)	Mass (Ton)		Mass (Ton)		
	6	3	6	3	6	3	3	1	3	1	3	1
0.7	G	N	G	G	G	G	N	N	G	N	G	N
0.5	N	N	G	N	G	G	N	N	N	N	G	N
0.3	N	N	N	N	G	G	N	N	N	N	N	N
0	N	N	N	N	N	N	N	N	N	N	N	N

G=Global plastic failure, N=No failure,

Table 11: Failure modes for column section UC 305×305×118

L=4m Impact Location 1.5 m							L=4m, Impact Location = 1 m					
(P/P <sub>Design</sub> ) %	Impact velocity (km/h)						Impact velocity (km/h)					
	20		40		80		20		40		80	
	Mass (Ton)		Mass (Ton)		Mass (Ton)		Mass (Ton)	Mass (Ton)		Mass (Ton)		
	6	3	6	3	6	3	3	1	3	1	3	1
0.7	G+FD	N	G+FD	G+FD	S	G+FD	G+FD	N	G+FD	G+FD	G+FD	G+FD
0.5	G+FD	N	G+FD	G+FD	G+FD	G+FD	N	N	G+FD	N	G+FD	G+FD
0.3	N	N	G+FD	N	G+FD	G+FD	N	N	N	N	G+FD	G
0	N	N	G	N	G+FD	G+FD	N	N	N	N	N	N

G=Global plastic failure, S =Shear failure, N=No failure, G+FD=Global plastic failure + local flange distortion

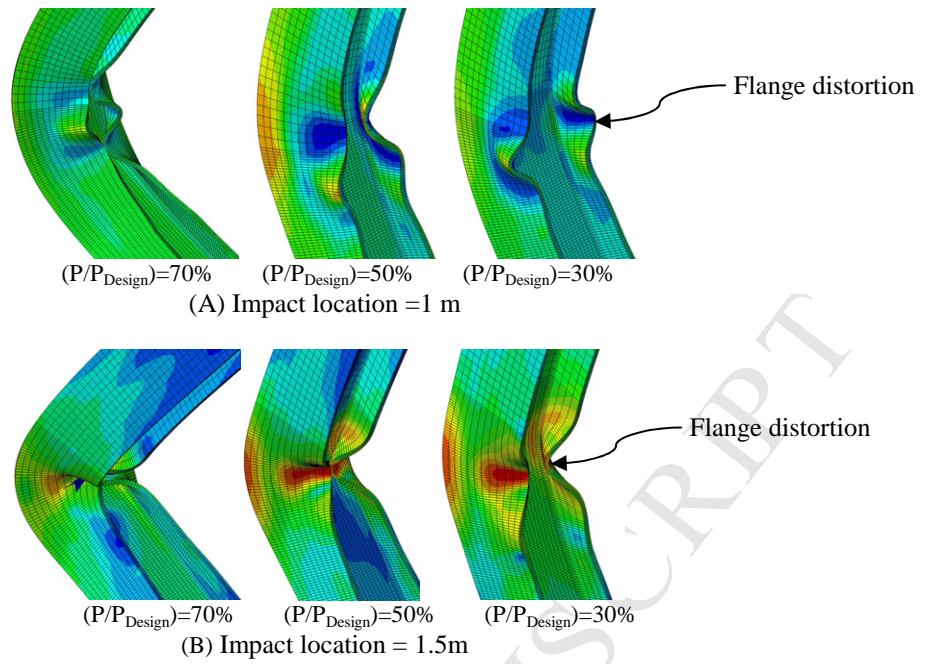


Figure 17: Local flange distortion at the impact zone for the section UC305 $\times$ 305 $\times$ 118

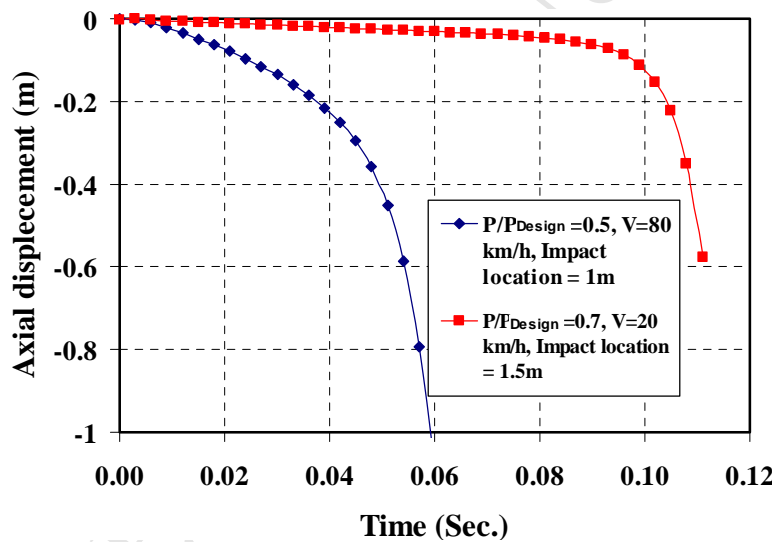


Figure 18: Axial displacement history for the two columns in Figure 16

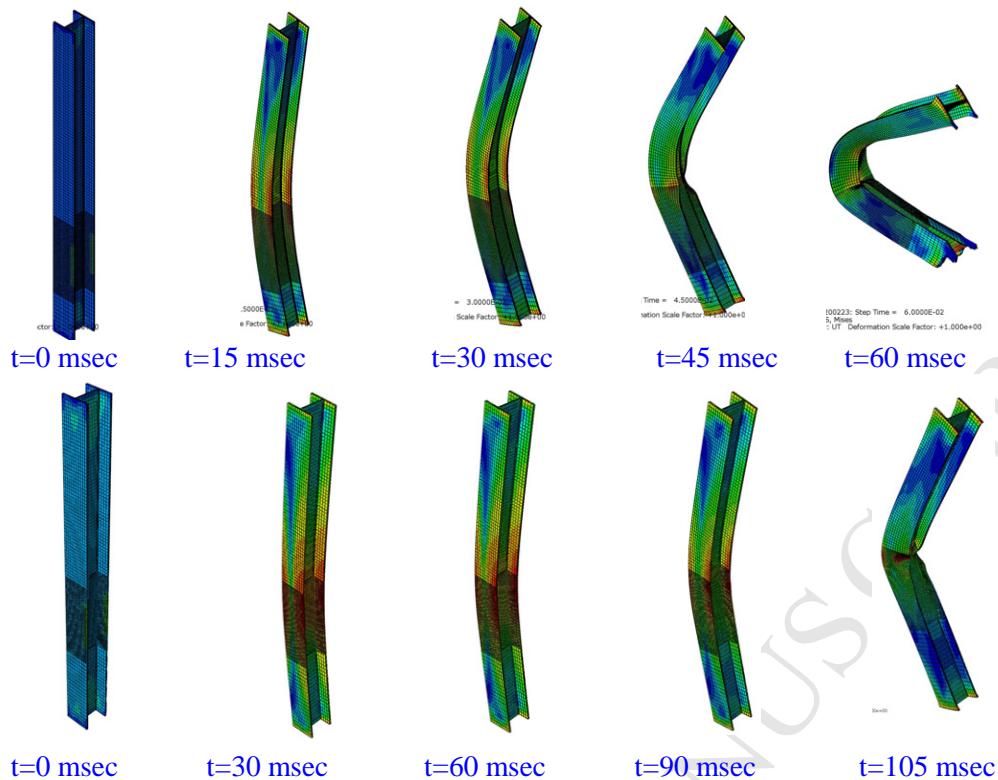
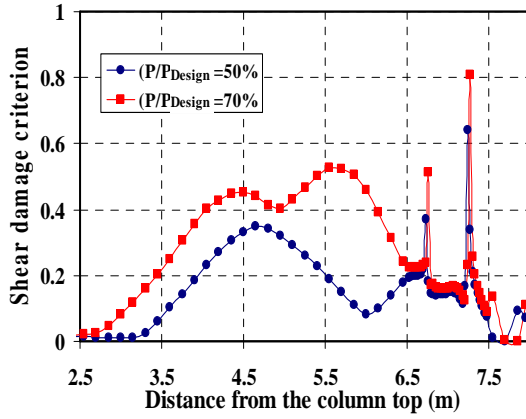
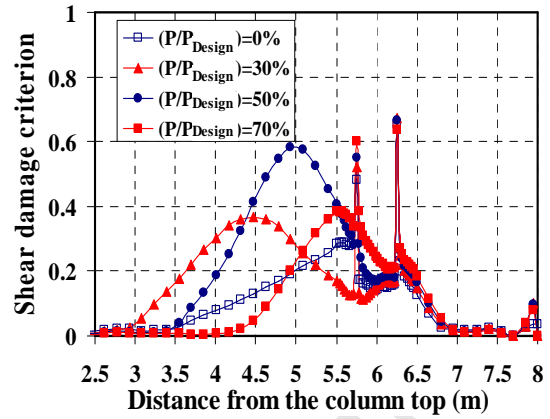


Figure 19: Deformed shape history of column section UC 305 $\times$ 305 $\times$ 118; Top: Impact location= 1.0 m, P/P<sub>Design</sub> =0.5, Impact mass =1 Ton, Impact velocity =80 km/h; Bottom: Impact location= 1.5 m, P/P<sub>Design</sub> =0.7, Impact mass =3 Ton, Impact velocity =20 km/h

Figures 18 and 19 show shear damage profiles along the column height for the two columns that are most vulnerable to shear failure due to the high impacting mass and velocity [11, 12]. It can be seen that apart from two cases which have shown high tendency to local shear failure, the damage initiation criteria were much lower than 1.0. It is apparent from these figures that the transverse shear failure is unlikely to occur in the transversely impacted steel column when the transverse impact speed is within the range of low to intermediate velocities.

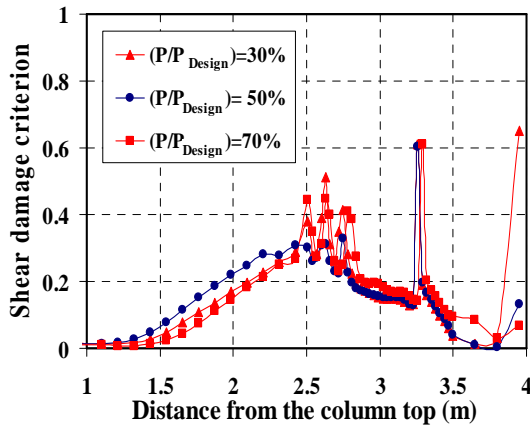


(A) Impact location = 1 m, impact mass = 3 Ton,

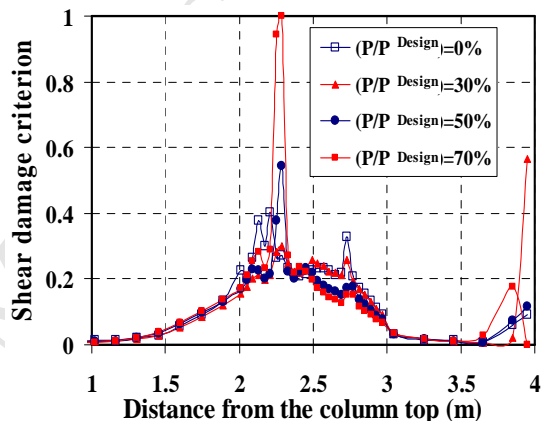


(B) Impact location = 2 m, impact mass = 6 Ton

Figures 20: Shear damage initiation criterion profile along column length for section UC 356×406×340, impact velocity = 80km/h



(A) Impact location = 1 m, impact mass = 3 Ton



(B) Impact location = 1.5 m, impact mass = 6 Ton

Figures 21: Shear damage initiation criterion profile along column length for section UC305×305×118, impact velocity = 80km/h

### 3.5.2 Impact energy

The most simplistic analytical method for columns subjected to transverse impact loads would be to assume quasi-static behaviour. This approach is based on the energy balance principle and the most important parameter for the impactor is its kinetic energy. To investigate this assumption, the numerical simulations considered a constant level of impact energy, but different combinations of impactor mass and velocity. Figures 20(A) and 20(B) present the column behaviour for two different levels of impact kinetic energy (KE).

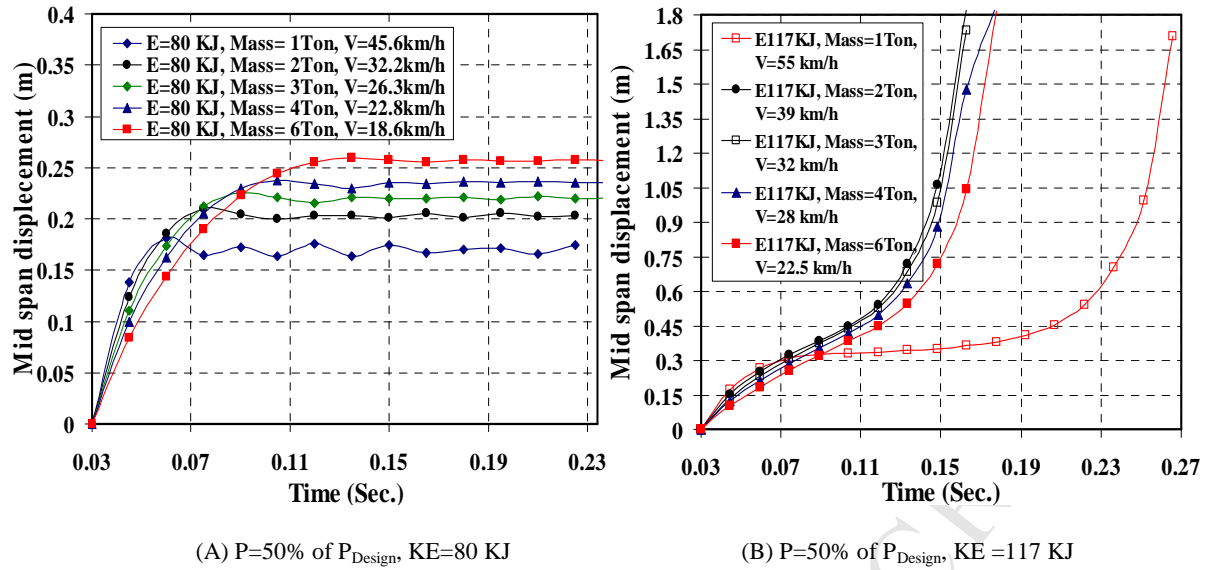


Figure 22: Column (section UC 305×305×118, L=4 m, impact location = 1 m,  $P/P_{Design}=50\%$ ) behaviour under the same impact energy but with different combinations of impactor mass and velocity

It can be noticed from Figure 20 that in both cases, the deformation behaviour of the same column under the same level of external impact energy but different combinations of impact mass and velocity are different. Both Figures indicate that a smaller velocity tends to give more severe column response (larger displacement). Nevertheless, whether or not the impacted column would fail (which is the most important design decision) appear not to be very sensitive to different values of the impact mass and velocity as long as the external impact energy is the same. For example, in Figure 20(A), the impact energy of 80 KJ was about 70% of the critical impact energy to cause column failure. Therefore, none of the columns experienced failure. In contrast, in Figure 20(B), the impact energy of 117 KJ was at the level of critical impact energy of the column. All cases indicate column failure even though the case with the highest velocity 55km/hour took longer time for the column to reach failure.

This may be confirmed by studying the change in kinetic energy of the column. Figure 21 presents the total kinetic energy histories of the whole structural system, including both the

column and the impactor, for columns subjected to the critical impact energy (117 KJ) but with different combinations of impactor mass and velocity under an axial compressive load of 50% of the design load. From this figure it can be seen that for all combinations, the total kinetic energy decreases after impact due to increasing strain energy in the column. After reaching the minimum value, the total kinetic energy increases. This increase is caused by accelerated movement of the column, indicating the column losing its stability.

After impact, if the column is stable, the kinetic energy of the system will become zero when both the column and the impactor come to rest. In contrast, if the column fails after impact, then the column will accelerate in deformation and the kinetic energy will increase. For the column at the critical situation, its kinetic energy will decrease to zero and but will then increase. The energy histories of these three situations are exemplified in Figure 22. According to the trend shown in Figure 22, the results in Figure 21 suggest that only one column was at the critical situation while all other columns lost global stability without coming to rest. The difference in behaviour of these columns is mainly due to different amounts of energy absorption of these columns as a result of their difference in deformation pattern under different combinations of impactor mass and velocity (thus different momentum when keeping the impact energy the same). Nevertheless, the minimum total kinetic energies of these columns were only a small fraction of the initial total kinetic energy. Therefore, it may be accepted that the column deformation patterns are very similar. This will lead to considerable simplification to aid development of an analytical model for calculation of the critical velocity of impact that will just cause the column to fail.

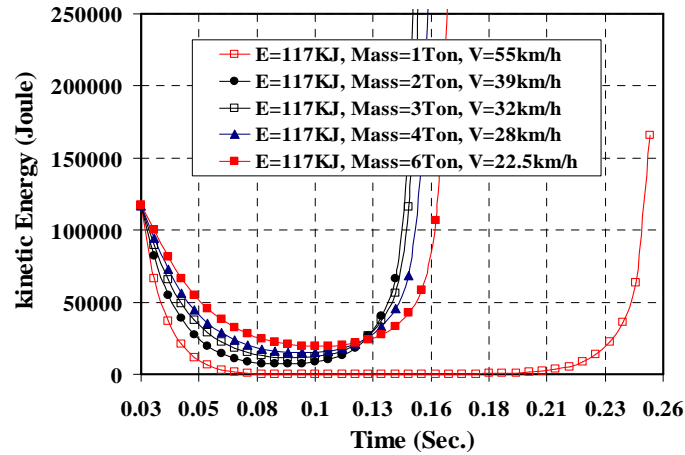


Figure 23: Kinetic energy history of the axially loaded steel column (section UC 305×305×118, L=4 m, impact location =1m,  $P/P_{Design}=50\%$ , Impact energy = 117KJ)

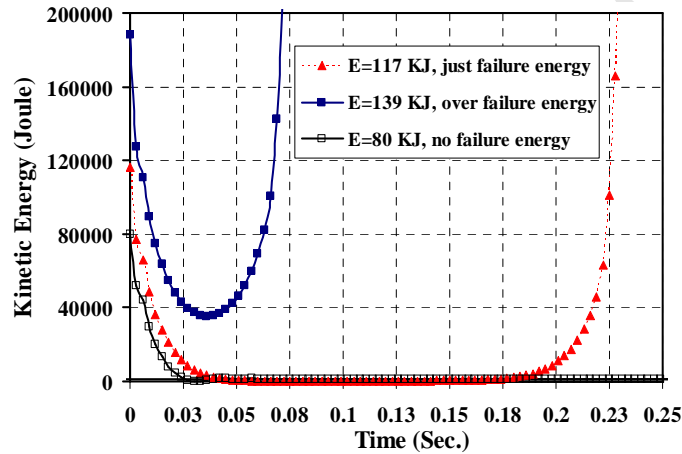


Figure 24: Comparison of total kinetic energy history of columns without failure, at the critical condition, with clear failure

### 3.5.3 Plastic hinge location

When developing analytical solutions to the problem, it will be necessary to know where the plastic hinge forms so as to quantify the plastic dissipation energy of the column. Figure 23 shows how the relationship between the axial compressive load as a percentage of the design load (vertical axis) and the location of the plastic hinge, measured from the column base, as a percentage of the total column length, for columns failed in global mode for the two column lengths and different impact locations.

Figures 23 and 24 show that the plastic hinge location is not significantly effected by the axial load values or the impact location because it is always close to the column mid-span (0.375-0.5)L. This is because when the column fails by global plastic instability, the deformation shape of the column is more likely to follow the first mode for static buckling [17], especially for high levels of axial compressive load ( $> 30\%P_{design}$ ).

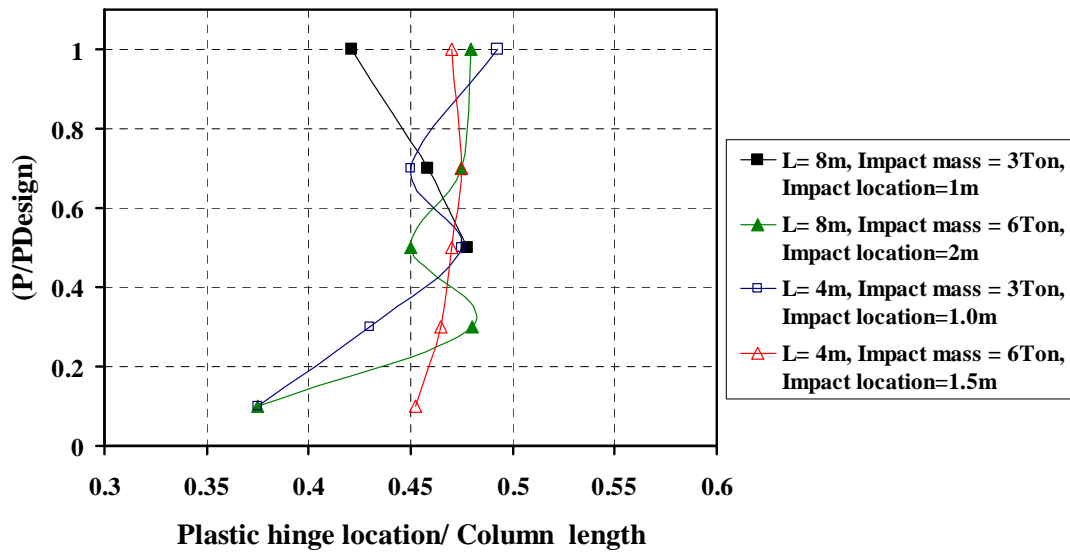


Figure 25: Locations of plastic hinge measured from column base for different axial load ratios

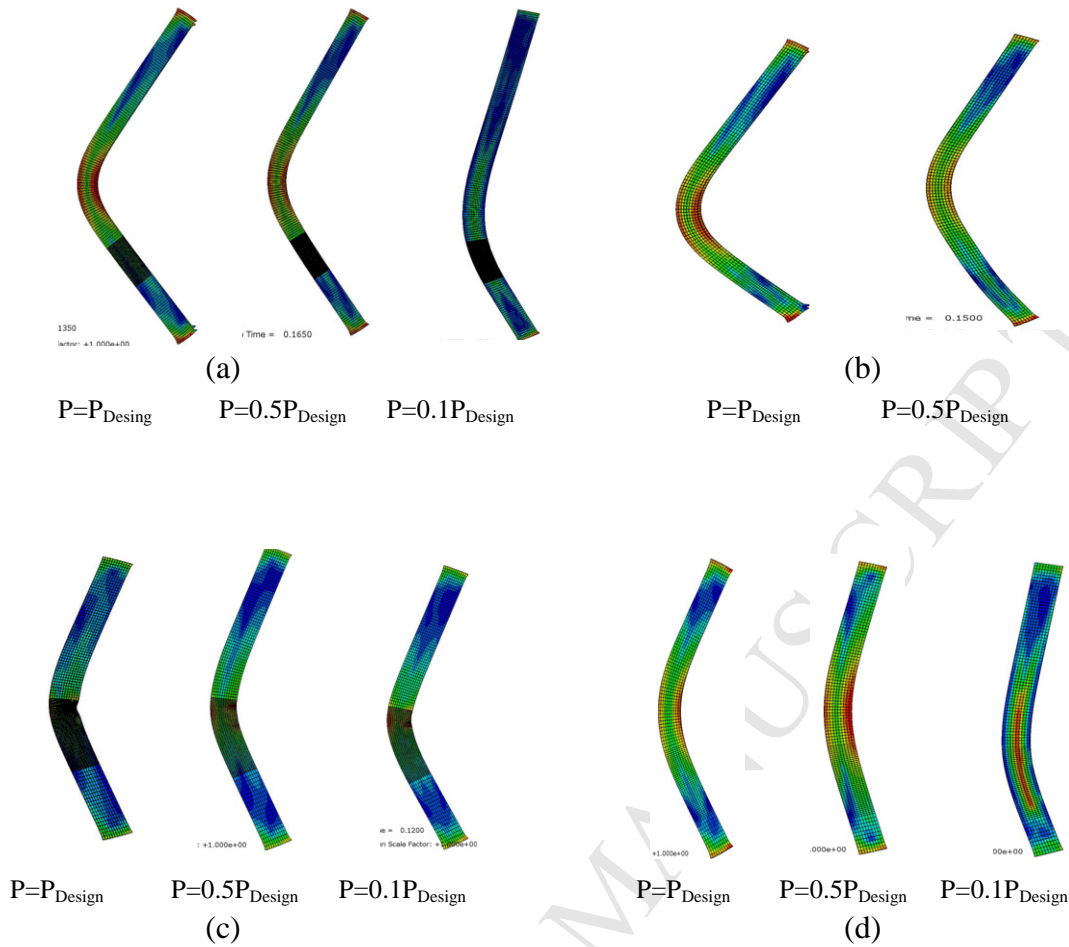
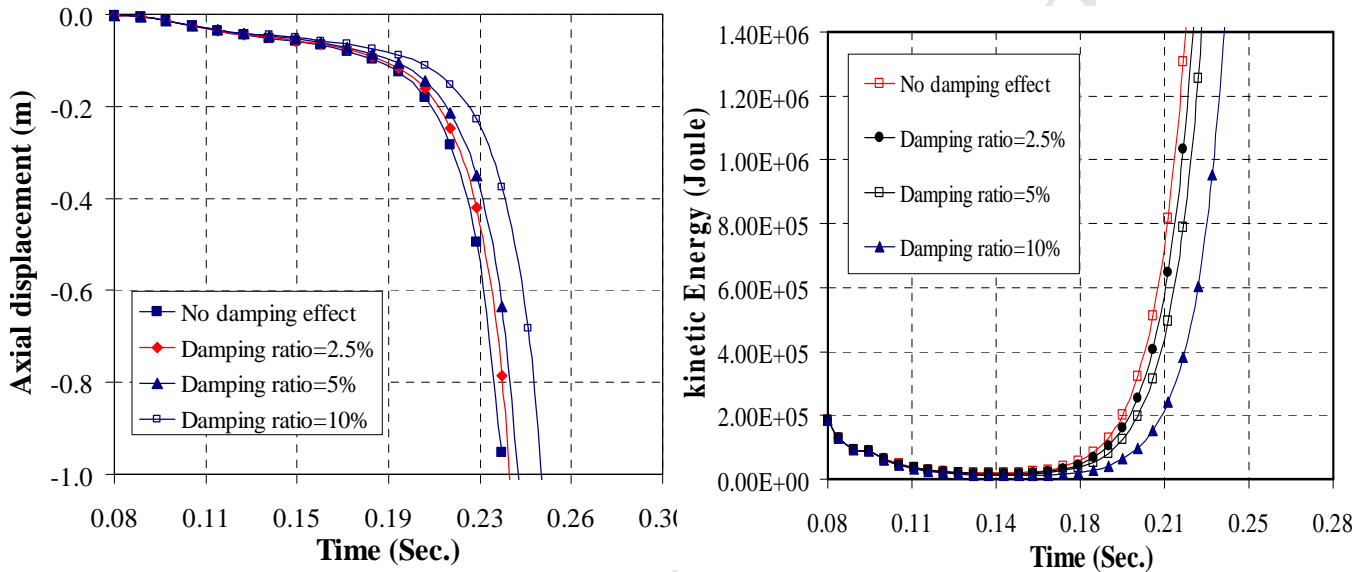


Figure 26: Collapse shape showing locations of plastic hinge for different axial load ratios (a)  $L = 8$  m, impact location = 2 m, Mass = 6 Ton; (b)  $L = 8$  m, impact location = 1 m, Mass = 3 Ton; (c)  $L = 4$  m, impact location = 1.5 m, Mass = 6 Ton ; (e)  $L = 4$  m, impact location = 1 m, Mass = 3 Ton

### 3.6 Damping effects

The numerical simulations presented in sections 2.1-2.3 have not considered damping effects but the simulation results still show good correlation with the experimental results. This indicates that damping have no significant effect on the structural behaviour. This is expected because the interest of this study is in column structural behaviour unto to the point of failure. During this stage, the impact duration is very short compared to the natural period of the structure system (Jones [19], Sastranegara et a, [18], Zeinodini, et al, [16] and Thilakarathna

et al, [24]). Nevertheless, to confirm this assumption, three damping ratios (2.5%, 5% and 10%) were introduced into one of the parametric case studies. The damping ratio was defined using Raleigh mass proportional damping coefficient since it is the most suitable procedure for dynamic explicit analysis [20]. Figure 27 compares the simulation results in terms of the column axial displacement at the top and kinetic energy histories.



(A) Column top axial displacement–time history (B): Kinetic energy-time history

Figure 27: Effects of damping on the behaviour of a steel column (section UC 356×406×340, L=8 m, impact location = 2 m,  $P/P_{Design}=70\%$ ).

As can be seen from Figure 14(A) and 14(B), the material damping ratio had only marginal effect on the column behaviour, showing no effect on whether or not the column would fail (which is the most important objective of this research) and a slight delay in column failure time when compared to the reference case of no damping.

#### 4. SUMMARY AND CONCLUSIONS

This paper has presented the results of a numerical study to validate an ABAQUS/Explicit model to simulate the behaviour and different failure modes of steel members subjected to lateral impact. The ABAQUS/Explicit model is able to capture the modes of global buckling of steel columns under compression, shear and support tension tearing. Afterwards, the validated numerical model was used to conduct a parametric study to investigate the effects of several parameters on the behaviour and failure modes of axially pre-loaded steel columns subjected to transverse impact. From the results of this parametric study, the following conclusions may be drawn:

- (1) The predominate failure mode for axially unrestrained compressed columns under transverse impact was global buckling of the column.
- (2) Some column failure involved large local flange distortion. However, this local flange distortion is a result, not cause, of global column failure.
- (3) Column failure was primarily dependent on the level of impact kinetic energy. At the same impact kinetic energy, different values of impactor mass and velocity had minor effect on column failure.
- (4) Except for very low level of axial compression (<25% design resistance), the formation of plastic hinge was almost independent of the impact position, with the plastic hinge location being close to the centre of the column.

#### REFERENCES

- [1]. B.R. Ellis, P.J. Dillon, Road vehicle impacts on buildings in the uk - Regulation and risk, *The Structural Engineer*, Vol. 81, 2003, pp 36-40.

- [2]. A. Ghose, Strategies for the management of bridges for vehicular impacts, *Structures and Buildings*, Vol. 162, 2009 pp. 3-10.
- [3]. BS 6399: Part 1: British Standard. Loading For Buildings. Part 1. Code of Practice For Dead And Imposed Loads, 1996.
- [4]. EN 1991-1-7:2006, Eurocode 1 - Actions on structures - Part 1-7: General Actions & Accidental actions. Irish standards, 2006.
- [5]. European Prestandard ENV 1991-2-7:1997. Eurocode 1: Part 2-7: Accidental actions due to impact and explosion. June 1998.
- [6]. Network Rail and the Highways Agency (HA), BD 60/04.
- [7]. S.B. Menkes, H.J. Opat, Broken beams, *Experimental Mechanics*, Vol. 13, 1973, pp. 480-486.
- [8]. F.L. Chen, T.X. Yu, Influence of Axial Pre-Load on Plastic Failure of Beams Subjected to Transverse Dynamic Load, *Key Engineering Materials*, Vol. 117-180, 2000, pp. 255-260.
- [9]. J. Liu, N. Jones, Experimental investigation of clamped beams struck transversely by a mass, *International Journal of Impact Engineering*, Vol. 6, 1987, pp. 303-335.
- [10]. J. Yu, N. Jones, Numerical simulation of a clamped beam under impact loading, *Computers & Structures*, Vol. 32, 1989, pp. 281-293.
- [11]. J. Liu, N. Jones, Further experimental investigations on the failure of clamped beams under impact loads, *International Journal of Solids and Structures*, Vol. 27, 1991, pp. 1113-1137.
- [12]. J. Yu, N. Jones, Numerical simulation of impact loaded steel beams and the failure criteria, *International Journal of Solids and Structures*, Vol. 34, 1997, pp. 3977-4004.
- [13]. M.N. Mannan, R. Ansari, H. Abbas, Failure of aluminium beams under low velocity impact, *International Journal of Impact Engineering*, Vol. 35, 2008, pp. 1201-1212.
- [14]. M.R. Bambach, H. Jama, X.L. Zhao, R.H. Grzebieta, Hollow and concrete filled steel hollow sections under transverse impact loads, *Engineering Structures*, Vol. 30, 2008, pp. 2859-2870.

- [15]. Zeinoddini, G.A.R. Parke, J.E. Harding, Axially pre-loaded steel tubes subjected to lateral impacts: an experimental study, *International Journal of Impact Engineering*, Vol. 27, 2002, pp. 669-690.
- [16]. M. Zeinoddini, J.E. Harding, G.A.R. Parke, Axially pre-loaded steel tubes subjected to lateral impacts (a numerical simulation), *International Journal of Impact Engineering*, Vol. 35, 2008, pp. 1267-1279.
- [17]. T. Adachi, T. Tanaka, A. Sastranegara, A. Yamaji, S.-K. Kim, I.-Y. Yang, Effect of transverse impact on buckling behavior of a column under static axial compressive force, *International Journal of Impact Engineering*, Vol. 30, 2004, pp. 465-475.
- [18]. A. Sastranegara, T. Adachi, A. Yamaji, Effect of transverse impact on buckling behavior of compressed column, *Thin-Walled Structures*, Vol. 44, 2006, pp. 701-707.
- [19] N. Jones, *Structural Impact*. 2nd ed. Cambridge University Press, 1997.
- [20]. SIMULIA, “:Abaqus analysis User’s Manual Ver. 6.8-2”, Vol. 3 and Vol.5, Providence, Rhode Island, 2008.
- [21]. BS 5950, British Standard – Structural Use of Steelwork in Building: Part 1: Code of Practice for Design – Rolled and Welded Sections. London: British Standards Institution, 2001.
- [22] EN1993-1-1. Eurocode 3 Design of steel structures. General rules and rules for buildings. 2005.
- [23]. [http://www.roymech.co.uk/Useful\\_Tables/Sections/UCA\\_dim\\_prop.html](http://www.roymech.co.uk/Useful_Tables/Sections/UCA_dim_prop.html), 15/10/2010
- [24] H.M.I. Thilakarathna, D.P. Thambiratnam, M. Dhanasekar, N. Perera, Numerical simulation of axially loaded concrete columns under transverse impact and vulnerability assessment, *International Journal of Impact Engineering*, Vol.37, 2010, pp. 1100-1112
- [25] S. P. Timoshenko, J. M. Gere, *Theory of Elastic Stability*. 2nd ed. McGraw-Hill, NY., 1961.